metals

MDPI

Review

Constitutive Models for the Strain Strengthening of Austenitic Stainless Steels at Cryogenic Temperatures with a Literature Review

Bingyang He [1], Juan Wang [1,*] and Weipu Xu [2]

[1] Key Laboratory for Liquid-Solid Structural Evolution and Processing of Materials (Ministry of Education), Shandong University, Jinan 250061, China; 18337656719@163.com
[2] Shanghai Institute of Special Equipment Supervision and Inspection Technology, Shanghai 200062, China; neiltwo@126.com
* Correspondence: jwang@sdu.edu.cn

Abstract: Austenitic stainless steels are widely used in cryogenic pressure vessels, liquefied natural gas pipelines, and offshore transportation liquefied petroleum gas storage tanks due to their excellent mechanical properties at cryogenic temperatures. To meet the lightweight and economical requirements, pre-strain of austenitic stainless steels was conducted to improve the strength at cryogenic temperatures. The essence of being strengthened by strain (strain strengthening) and the phase-transformation mechanism of austenitic stainless steels at cryogenic temperatures are reviewed in this work. The mechanical properties and microstructure evolution of austenitic stainless steels under different temperatures, types, and strain rates are compared. The phase-transformation mechanism of austenitic stainless steels during strain at cryogenic temperatures and its influence on strength and microstructure evolution are summarized. The constitutive models of strain strengthening at cryogenic temperatures were set to calculate the volume fraction of strain-induced martensite and to predict the mechanical properties of austenitic stainless steels.

Keywords: austenitic stainless steel; strain strengthening; cryogenic temperature; phase transformation mechanism; mechanical properties; constitutive model

check for updates

Citation: He, B.; Wang, J.; Xu, W. Constitutive Models for the Strain Strengthening of Austenitic Stainless Steels at Cryogenic Temperatures with a Literature Review. *Metals* **2023**, *13*, 1894. https://doi.org/10.3390/met13111894

Academic Editors: Andrea Di Schino, Damien Fabrègue and Claudio Testani

Received: 16 October 2023
Revised: 7 November 2023
Accepted: 9 November 2023
Published: 15 November 2023

1. Introduction

The crystal structure of austenitic stainless steel exhibits a face-centered cubic structure (FCC), which has a higher density than that of a body-centered cubic crystal structure (BCC). The corrosion resistance of austenitic stainless steel is significantly good, making it one of the most widely used stainless steels in industrial production [1,2]. The face-centered cubic structure has four groups of slip surfaces and three slip directions on each group of slip surfaces. The 12 slip systems reduce the good plasticity and toughness of austenitic stainless steel. The yield strength of austenitic stainless steels at room temperature is 313.09 MPa, the tensile strength is 804.59 MPa, the yield strength at cryogenic temperature (−196 °C) is 558.91 MPa, and the tensile strength is 1633.52 MPa [3]. Therefore, the application of austenitic stainless steels in cryogenic temperature service equipment, such as cryogenic pressure vessels, liquefied natural gas pipelines, and offshore transportation liquefied petroleum gas storage tanks, often requires a large thickness for safety factors. As a result, the manufacturing cost and weight of the equipment increase, which does not meet the lightweight and economical requirements.

A significant feature of austenitic stainless steel is that it can be strengthened with strain. This phenomenon is called strain strengthening, which is obvious with a decrease in temperature or an increase in deformation during tensile strain. The main reason is the partial phase transformation from austenite to martensite, and the morphology and content of martensite play a key role in strain strengthening at cryogenic temperatures [4].

The thermodynamics required for the phase transformation from austenite γ to martensite α' is shown in Figure 1 [5]. The phase transformation mainly occurs in one of the following three ways: (a) temperatures below the critical temperature M_s, (b) temperatures above M_s while elastic stress provides kinetic phase transformation, or (c) temperatures above M_s while plastic tensile force provides kinetic phase transformation. Under different temperature conditions, there will be different proportions of austenite to martensite during the phase-transformation process. In addition to the macroscopic deformation caused by plastic strain, the process is accompanied by an increase in the phase volume, resulting in microstructural evolution.

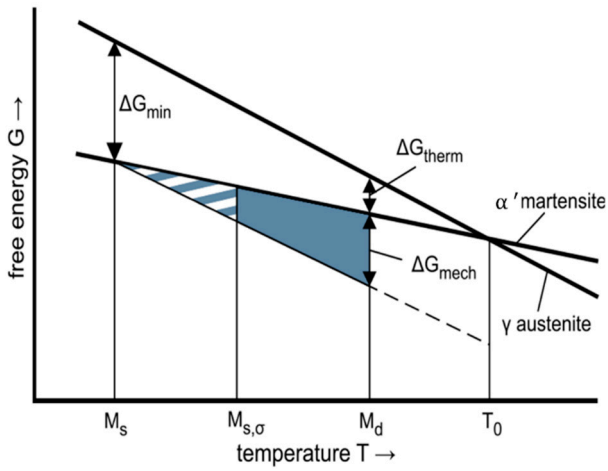

Figure 1. Austenite to martensite phase-transformation free energy (Reprinted from Ref. [5]).

The stress-assisted phase transformation in austenitic stainless steels only occurs when the temperature is close to absolute zero, and the phase transformation is less. The plastic strain-induced phase transformation does not have strict conditions, but it is the main mechanism in austenitic stainless steels [6]. Fewer phase transformations occur when the elastic stress provides kinetic phase transformation because it belongs to the stress-assisted phase transformation process. The strain or deformation-induced phase transformation belongs to the plastic strain-induced phase transformation process. During strain-induced phase transformation, austenite γ (FCC) is not directly transformed into α' (BCC) martensite but into mesophase ε (HCP) austenite [7]. Therefore, the main phase transformation formed during strain strengthening of austenitic stainless steels at cryogenic temperatures is plastic tensile-induced phase transformation.

In this work, recent studies on the strain strengthening of austenitic stainless steels at cryogenic temperatures are reviewed. The influence of strain conditions on mechanical properties at cryogenic temperatures and the phase-transformation mechanism are introduced. The two constitutive models for the simulation of microstructure evolution and mechanical property models for predicting the volumes of phase transformation are summarized.

2. Effect of Strain Conditions on Mechanical Properties

To maximize the mechanical properties of austenitic stainless steels at cryogenic temperatures, research on different aspects has been carried out, including retained austenitic stability [8,9], martensitic content [10–12], grain size of retained austenite and martensite [13,14] and temperatures and methods of strain [15,16]. The effect of cryogenic conditions and strain types on the mechanical properties of austenitic stainless steels is included in this review.

2.1. Effects on the Mechanical Properties of 316 Steel

The effect of strain on the mechanical properties of 316L steel (L-PBF316) prepared by Laser Powder Bed Fusion was studied, and the results showed that the yield strength 594 MPa and tensile strength 689 MPa at 20 °C increased to 751 MPa and 1403 MPa at −196 °C with a decrease in elongation from 49% to 41% [17]. The 316LN steel experienced the pre-strain of 15%, 25%, and 35% at 20 °C, −196 °C, and −268.8 °C, indicating a significant improvement of the yield strength and the tensile strength under a loading rate of 1.0 mm/min (shown in Table 1) [18]. The yield strength increased by 199.6%, 72.5%, and 91.5%. The tensile strength increased by 84.9%, 33.8%, and 34.5%. The yield ratio increased by 61.7%, 28.8%, and 42.3% at 20 °C, −196 °C, and −268.8 °C when the amount of pre-strain increased from 0% to 35%. The influence of pre-strain and temperatures on mechanical properties is shown in Figure 2. Accordingly, the percentage of α' martensite increased sharply at cryogenic temperatures (−196 °C and −268.8 °C) with more dislocations.

Table 1. Tensile properties of 316LN steel under different pre-strain strengthening processes. Reproduced with the permission from [18], [S. Wu et al.], [Cryogenics]; published by [Elsevier Ltd., Amsterdam, The Netherlands], [2022].

Amount of Pre-Strain/%	Test Temperature /°C	Yield Strength /MPa	Tensile Strength /MPa	Elongation/%	Yield Ratio
0	20	270	598	68	0.452
15	20	513	799	25	0.642
25	20	636	947	9	0.672
35	20	809	1106	4	0.731
0	−196	672	1311	70	0.513
15	−196	933	1493	55	0.625
25	−196	1030	1615	44	0.638
35	−196	1159	1754	33	0.661
0	−268.8	832	1536	55	0.542
15	−268.8	1063	1740	36	0.611
25	−268.8	1301	1883	29	0.691
35	−268.8	1593	2066	19	0.771

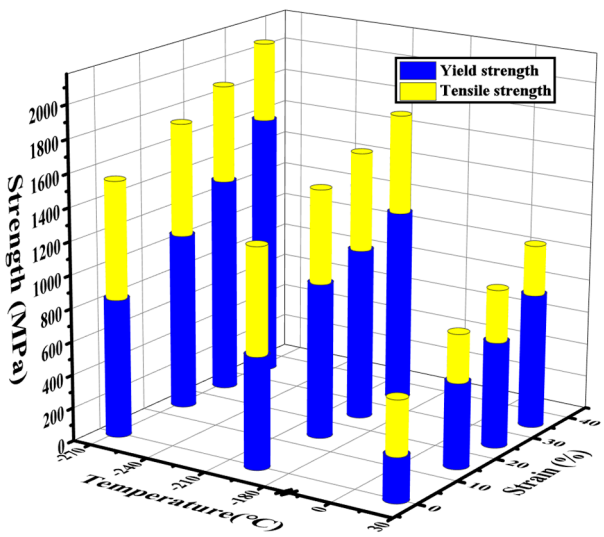

Figure 2. Influence of pre-strain and temperatures on the mechanical properties of 316LN.

The strength of metastable austenitic stainless steels is improved by experiencing cyclic pre-strain at −196 °C while maintaining the high elongation [19]. The phase transformation-induced plastic effect (TRIP) plays a full role in the tensile process. The cyclic plastic strain

changes the characteristics of rapid phase transformation after full nucleation, which makes the reinforced microstructure maintain the phase transformation ability. Twin deformation, phase transformation, and serrated yield of 316L steel are difficult to occur when in-situ, small-scale, or high-strain deformation is conducted at −196 °C and −268.8 °C [20]. This is because austenite deforms through twin crystals at low temperatures and low strain by TEM observation. The results of uniaxial tensile and cyclic strain tests on 316L (MASS) at −196 °C showed that the yield strength and tensile strength increased with a decrease in elongation from 65% to 49% [21]. Observed by field emission scanning electron microscopy, the fracture morphology of L-PBF316L steel showed that the tensile strength was improved, and the elongation was preserved 55% at −196 °C [22]. The yield strength and tensile strength of 316 steel increased from 399.6 MPa and 851.2 MPa at −50 °C to 470 MPa and 1160.5 MPa at −130 °C under a loading rate of 2.0 mm/min [23].

2.2. Effect on the Mechanical Properties of 304 Steel

Table 2 shows the mechanical properties of 304 steel after multi-pass cold rolling at different temperatures with a crosshead velocity of 0.5 mm/min [24]. The strength increases with a decrease in temperature or an increase in deformation. In particular, the strength of 304 steel after a multi-pass rolling of 20% at −196 °C is much higher than that of 0 °C, and it is increased by 802 MPa (shown in Figure 3). The yield strength, the tensile strength, and the yield ratio increase with an increase in rolling deformation due to martensitic transformation.

Table 2. Tensile properties of 304 steel under different multi-pass cold rolling processes. Reproduced with the permission from [24], [P. Mallick et al.], [Mater. Charact.]; published by [Elsevier Ltd., Amsterdam, The Netherlands], [2017].

Multi-Pass Cold Rolling/%	Test Temperature /°C	Yield Strength /MPa	Tensile Strength /MPa	Elongation /%	Yield Ratio
/	20	259	675	90	0.384
10	0	703	930	20	0.756
20	0	742	981	30	0.756
30	0	834	1098	40	0.760
40	0	936	1225	10	0.764
10	−196	1061	1306	20	0.812
20	−196	1463	1589	20	0.921

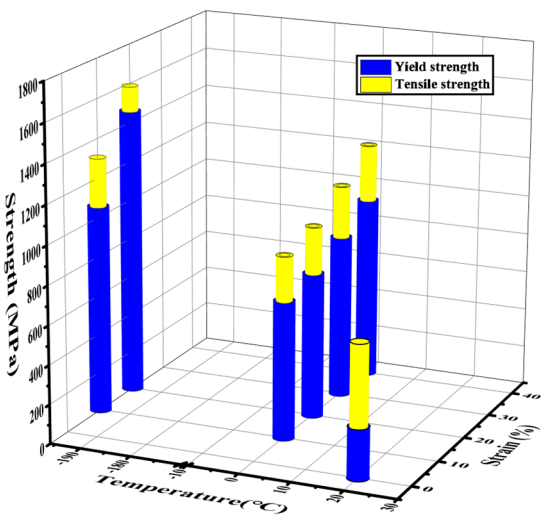

Figure 3. Influence of multi-pass cold rolling on tensile properties of 304 steel.

A total of 304 cylindrical rods with a gradient phase are obtained by torsion at −196 °C [25]. A good combination of strength and plasticity was achieved when austenite gradually decreased, with martensite occurring by the strain gradually increasing from the center of the cylinder to the edge due to the higher fraction of ε/α'. By comparing the stress–strain curve of 25% pre-strain at 0 °C, −20 °C, −40 °C, −80 °C, −120 °C and −196 °C, the yield strength and tensile strength of 304 increased with a decrease in temperatures [26]. However, the tensile experiments of Fe-19Cr-3Mn-4Ni-0.15C-0.17N austenitic steel with different strains at −40 °C and −196 °C indicates that the tensile strength decreases when the strain and temperatures reach a certain value [27]. The tensile strength and impact toughness of 304 steel and its welded joints at cryogenic temperatures increased with an increase in deformation and a decrease in strain temperatures [28]. Strain-induced martensitic transformation plays a significant role in strain strengthening at cryogenic temperatures.

Table 3 shows the effects of strain conditions on the mechanical properties of austenitic stainless steels. The strain was conducted by static or cyclic tensile, torsional, or rolling deformation at low temperatures.

Table 3. Effects of strain conditions on the mechanical properties of austenitic stainless steels.

Strain Conditions	Material Type	Strain Rate /s^{-1}	Test Temperature /°C	Yield Strength /MPa	Tensile Strength /MPa	Elongation /%	Refs.
Static strain	316L	0.00025	−196	751	1403	41	[29]
	316L	—	−196	730	1080	56	[22]
	316L	—	−130	470	1160.5	40	[23]
	316L	—	−268.8	805	1200	28	[22]
Cyclic strain	304	0.005	−196	850	1800	25	[19]
	316L	0.001	−40	681	871	51.5	[29]
	316L	0.001	−80	700	920	72.7	[29]
Torsional strain	304	—	−196	1745	—	23	[25]
	304	—	−196	1147	1357	—	[30]
Rolling strain	304	—	−196	1463	1598	20	[17]
	304	0.0002	−196	2308.4	2165.9	23	[31]

3. Effect of Strain Conditions on Microstructure

Olson and Cohen proposed FCC → HCP, FCC → BCC, and other types of martensitic nucleation mechanisms, including crystal embryos at grain boundaries, sub-grain boundaries, and inclusion particle interfaces [32,33]. Martensitic transformation often arises accompanied by nucleation and growth processes. Nucleation defects are critical for the phase-transformation fraction of martensite [34]. Most martensitic transformations exhibit no thermal characteristics and are sustainable when temperatures decrease, and a small amount of isothermal martensitic transformations do not require cooling [35].

The influence of the original austenitic grain size on the autocatalytic phase transformation was studied with a thermodynamic model [36]. Phase-transformation activation energy decreases with an increase in driving force. The kinetics of the isothermal martensitic transformation of Fe-24Ni-3Mn alloy was analyzed by autocatalytic nucleation method [37]. The nucleation rate first increased and then decreased with the reaction time. The phase-transformation activation energy decreased with a decrease in temperatures. Grain boundaries provide most of the defects [38,39]. It is clarified that potential nucleation locations are required to excite and breed martensitic transformations, and then these fine grains contribute to the occurrence of martensitic transformations.

There are two methods of martensitic transformation. One is the direct transformation of austenite γ to α' martensite, and the other is the transformation of austenite γ to α' mesophase ε (HCP) martensite [32,33]. The $\gamma \rightarrow \alpha'$ is a common martensitic transformation

process [40,41]. The phase transformation of $\gamma \rightarrow \varepsilon \rightarrow \alpha'$ is mostly occurring in Fe-Mn alloy [42] and Fe-Cr-Ni alloy [43] with low stacking fault energy. Regarding the effect of ε on α' formation, it is reported that ε can provide potential nucleation locations to accelerate kinetic phase transformation [44]. However, ε is only a transitional phase [45] and not a prerequisite for the formation of α' [46]. The microstructure evolution of austenite grains after different cryogenic treatment times is shown in Figure 4 [47].

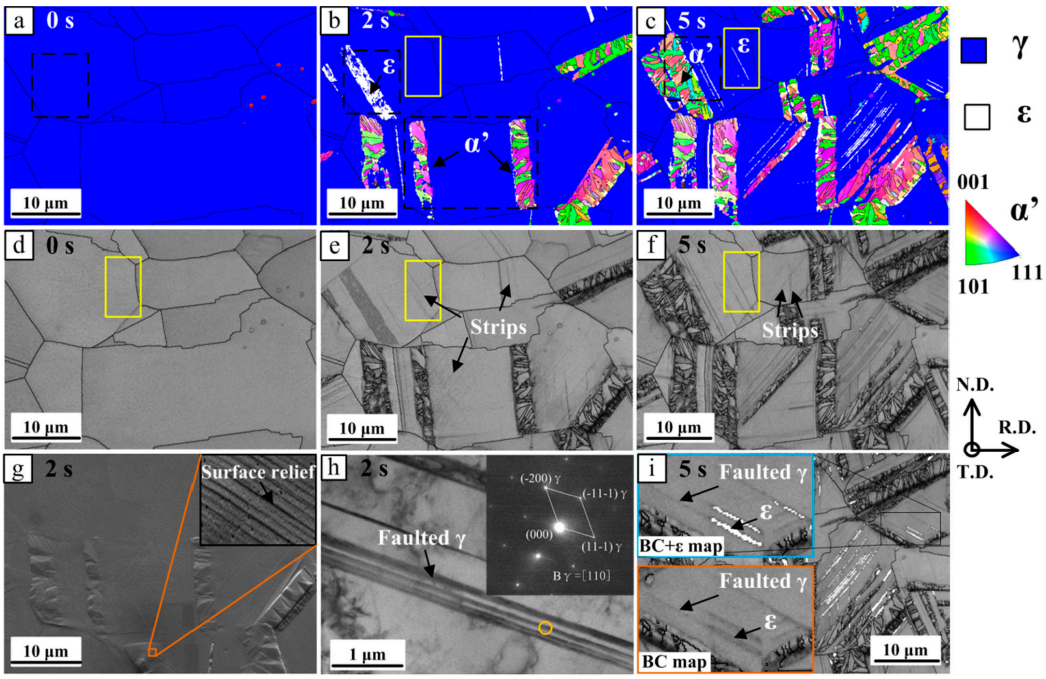

Figure 4. Microstructure evolution of specific regions after cryogenic treatment at 0, 2, and 5 s in liquid nitrogen (−196 °C). (**a**–**c**) EBSD method to obtain γ, ε phase diagram and α' orientation diagram. (**d**–**f**) Corresponding background contrast (BC) plot. (**g**) SEM image after 2 s. (**h**) TEM morphological image after 2 s and associated diffraction pattern of the yellow circle. (**i**) Diffraction image of ε phase and BC plot of EBSD after 5 s cryogenic treatment. Reproduced with the permission from [47], [J.L. Wang et al.], [Mater. Charact.]; published by [Elsevier Ltd., Amsterdam, The Netherlands], [2019].

Two transformation processes of $\gamma \rightarrow$ faulted $\gamma \rightarrow \varepsilon \rightarrow \alpha'$ and $\gamma \rightarrow$ faulted $\gamma \rightarrow$ stacking fault bundles $\rightarrow \alpha'$ were experimentally demonstrated in detail from Figure 4. In both, the martensitic transformation was always trigged first by faulted γ and then by ε and stacking fault bundles as transitions, eventually to the final α' transformation. These insights provide direct guidelines for explaining the martensitic transformation characteristics as well as further improving the martensitic transformation kinetic model.

The main phase transformation paths $\gamma \rightarrow \alpha$ in Fe-Cr-Ni alloys were only based on the position of α' slatted martensite in the final microstructure evolution after cryogenic treatment and the coexistence of ε martensite [43] or synchrotron diffraction (showing the approximate and predicted spatial positions of γ, ε and α' during in-situ cooling) [44]. Ref. [48] shows that the generation of the strips is directly related to the undulation of the specimen surface. This indicates the local plastic deformation to promote strips formed, and the TEM shows that the crystal structure is still face-centered cubic (FCC), indicating the existence of strips in γ faults. This suggests that ε nucleation in the current system follows a stacking fault mechanism [49]. The formation of stacking fault bundles under an applied stress is schematically illustrated in Figure 5 [50].

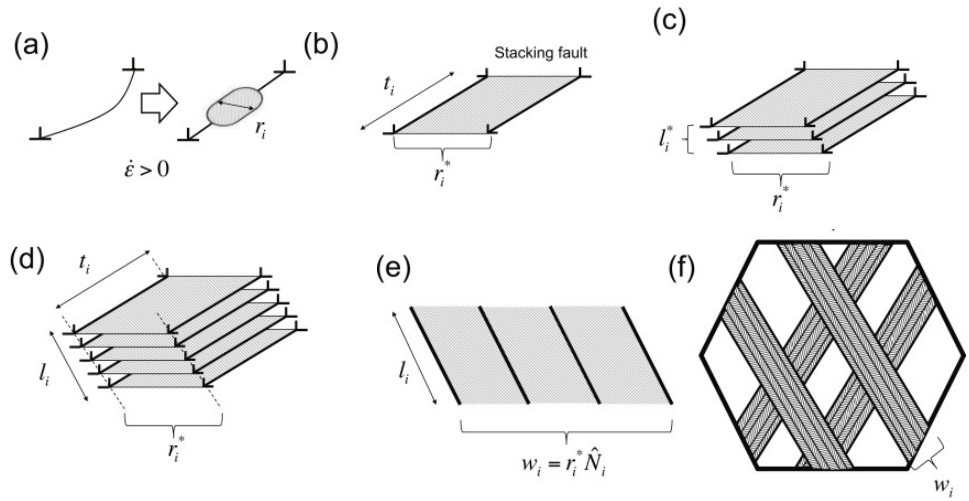

Figure 5. Schematic representation of the proposed mechanism of ε and twin formation [50]. (**a**,**b**) The size of the stacking fault increases with applied stress (positive strain rate $\dot{\varepsilon} > 0$) until reaching a critical width r_i^*, t_i is the thickness of a stacking fault, r_i is the width of a stacking fault. (**c**) The arrangement for a twin, l_i^* is a critical length. (**d**) The length of the embryo l_i increases and propagates through the grain interiors by subsequent overlapping of stacking faults in adjacent planes. (**e**) The width w_i increases by forming adjacent embryos of constant width r_i^*, $\hat{N}_i$ is the number of embryos in a band. (**f**) The formation of micro-bands. Reproduced with the permission from [50], [E. I. Galindo-Nava et al.], [Acta Mater.]; published by [Elsevier Ltd., Amsterdam, The Netherlands], [2017].

An isolated stacking fault first forms from a perfect dislocation under an applied stress. The size of the stacking fault increases with applied stress until it reaches a critical width. Then, several stacking faults overlap to form an embryo with critical width and length. The length of the embryo increases and propagates through the grain interiors by subsequent overlapping of stacking faults in adjacent planes. The increase in ε/twinning volume fraction increases by the formation and the overlapping of new embryos in various locations of grain, leading to the formation of micro-bands. This process aids in promoting the transformation of martensite [51].

4. Constitutive Models for Simulation of Microstructure Evolution and Mechanical Properties at Cryogenic Temperatures

A macroscopic constitutive model applicable to the plastic behavior of austenitic steels with strain-induced phase transformations was proposed [52], which is based on low elastic mode and large deformation equation. The effects of plastic strain, temperatures, and stress state on martensitic nucleation are mainly used to describe the elastic state and viscosity behavior of austenitic steels. The critical behavior of the alloy was investigated by the second-order phase transformation [53]. The strain-induced phase transformations are decomposed into plastic strain and volumetric strain. The phase transformation caused by plastic strain can be quantified experimentally, whereas the phase transformation caused by volumetric strain cannot be quantified. The experimental data from stress-assisted phase transformation is used to express the volumetric strain-induced phase transformation [52].

A model specific to cryogenic environments was proposed [53] and further enhanced with an anisotropic damage model [54], derived by generalizing Lemaitre's isotropic model to a tensor anisotropy model. It is assumed that the hardening coefficient of the austenitic matrix increases linearly with an increase in martensitic volume fraction in the model. The above models were transformed into a system constitutive model based on irreversible thermodynamics [55], in which dissipation phenomena are coupled through a dissipation potential. Lemaitre's isotropic model was modified to a form that clearly relies on the martensitic volume fraction generated after strain-induced phase transformation at cryogenic temperatures and the material coefficients that rely on the change in

martensitic volume fraction during phase transformation, resulting in dramatic material damage [56]. In finite element analysis of other constitutive models of strain-induced phase transformation at cryogenic temperatures [57–60], the results of damage evolution and crack propagation in austenitic stainless steels are also matched well with the results of strain experiments at cryogenic temperatures to maintain reliable accuracy.

Homayounfard et al. proposed a constitutive model of strain-induced phase transformation and material damage intensification at cryogenic temperatures based on continuous damage theory. The damage mechanism is based on large deformation dynamics and hyperelasticity, which combines the existing experimental results, considering the dissipation phenomenon caused by phase transformation and damage propagation during plastic deformation [6]. Damage softening and phase-transformation hardening occur, and they are also induced by strain at cryogenic temperatures. The Von Mises yield criterion (φ) for stainless steels during the strain process at cryogenic temperatures was modified, as shown in Equation (1) [6].

$$\varphi = \frac{\sqrt{3J_2(\tau)}}{1-D} - (K_0 + K_1\xi)r^n - \tau_y^0 \tag{1}$$

- J_2 is the second invariant of partial stress.
- D is the failure parameter.
- τ_y^0 is the initial yield stress.
- ξ is the martensitic volume fraction.
- K_0 is the initial pure austenitic hardening coefficient.
- K_1 is the additional coefficient of ξ.
- r is the hardening variable.

The experimental results show that the phase transformation of austenitic stainless steels begins simultaneously with the generation of damage initiation during strain at cryogenic temperatures, but the increase of martensitic volume fraction inhibits the increase of damage propagation [56]. By modifying the material parameters of the Lemaitre model, the damage potential function (ϕ^D) of austenitic stainless steel during strain-induced phase transformation at cryogenic temperatures is obtained [61], as shown in Equation (2).

$$\phi^D = \frac{S(\xi)}{(s+1)(1-D)}\left(\frac{Y}{S(\xi)}\right)^{s+1} \tag{2}$$

- $S(\xi)$: the material's ability to resist damage growth.
- D is the failure parameter.
- Y is the energy release rate.
- s is the Von Mises stress.

Considering the role of damage-nucleation strain, the damage growth ($\dot{D}$) is derived from the damage dissipation potential function, as shown in Equation (3).

$$\dot{D} = \frac{\dot{\gamma}}{(1-D)}\left(\frac{Y}{S(\xi)}\right)^{s} H(\varepsilon_P - \varepsilon_D) \tag{3}$$

- $\dot{\gamma}$ is the plastic multiplier.
- H is the step function.
- ε_P is the initial strain of plastic deformation.
- ε_D is the effect of damage-nucleation strain.

Since the dissipation phenomena during strain at cryogenic temperatures in stainless steels include plastic deformation, damage growth, and martensitic transformation, Homayounfard et al. superimposed the plastic variable potential function (ϕ^P), the failure growth potential function (ϕ^D) and the martensitic potential function (ϕ^{tr}) to obtain the dissipation potential (ϕ) in stainless steels after a strain at cryogenic temperatures [6], where

the plastic variable potential function (ϕ^P) is replaced by the modified Von Mises yield criterion (φ), as shown in Equation (4).

$$\phi = \left\{ \frac{\sqrt{3J_2(\tau)}}{1-D} - (K_0 + K_1\xi)r^n - \tau_y^0 \right\} + \left\{ \frac{S(\xi)}{(s+1)(1-D)} \left(\frac{Y}{S(\xi)} \right)^{s+1} \right\} + \phi^{tr} \quad (4)$$

The evolution of martensitic volume fraction has been described by empirical formulas, and the formula for the martensitic transformation potential function (ϕ^{tr}) has not been developed. It is assumed that the plastic spin is zero in the constitutive model of strain for stainless steels at cryogenic temperatures. The evolution of the plastic deformation gradient ($\overline{d^P}$) is determined by the rotational plastic deformation rate [6], as shown in Equation (5).

$$\overline{d^P} = \dot{\gamma}\frac{\partial \phi^P}{\partial \tau} = \dot{\gamma}N \quad (5)$$

- N represents the flow direction.
- τ represents the yield stress.

The cumulative plastic strain ($\dot{\overline{\varepsilon^P}}$), another important problem during strain of stainless steels at cryogenic temperatures, is also determined according to the rotational plastic deformation rate [56], as shown in Equation (6).

$$\dot{\overline{\varepsilon^P}} = \sqrt{\frac{2}{3}}\left\|\overline{d^P}\right\| = \frac{\dot{\gamma}}{(1-D)} \quad (6)$$

The model parameters of AISI304 steel were determined and corrected according to the results from the tensile test at −196 °C. The calculated results of the strain-induced phase transformation and damage propagation behaviors of AISI304 and AISI316L at −268.8 °C agree with the literature [56,60–63], as shown in Figure 6.

304L and 316L austenitic stainless steels retain 40~50% fracture strain under cryogenic conditions and have good ductility near absolute zero [31,64]. Therefore, it is particularly important to study the phase-transformation behavior induced by fracture strain of austenitic stainless steels at low temperatures. The nonlinear constitutive behavior of austenitic stainless steels 304 and 316 during the ultimate tensile strain at cryogenic temperatures was studied to set up the constitutive model for the cryogenic fracture strain-induced phase transformation of austenitic stainless steels by experiment and simulation [65–67].

Experimental and modeling studies of 316L austenitic stainless steel with symmetrical notches in liquid nitrogen (−196 °C) and liquid helium (−268.8 °C) environments were carried out in ref. [60]. The strain process at cryogenic temperatures is divided into two stages, no-hardening and linear hardening, where the initial flow stresses within each serration in the stress–strain curve of the non-hardening stage are the same, and an ideal plastic model is used, as shown in Equation (7).

$$f(\sigma_{ij}) = \sigma_i - \sigma_0(T) \quad (7)$$

- $f(\sigma_{ij})$ represents the plastic dissipation potential.
- σ_0 represents the flow stress depending on the temperature T.

σ_i can be determined by the bias stress (s_{ij}), as shown in Equation (8).

$$\sigma_i = \sqrt{\frac{3}{2}}|s_{ij}| \quad (8)$$

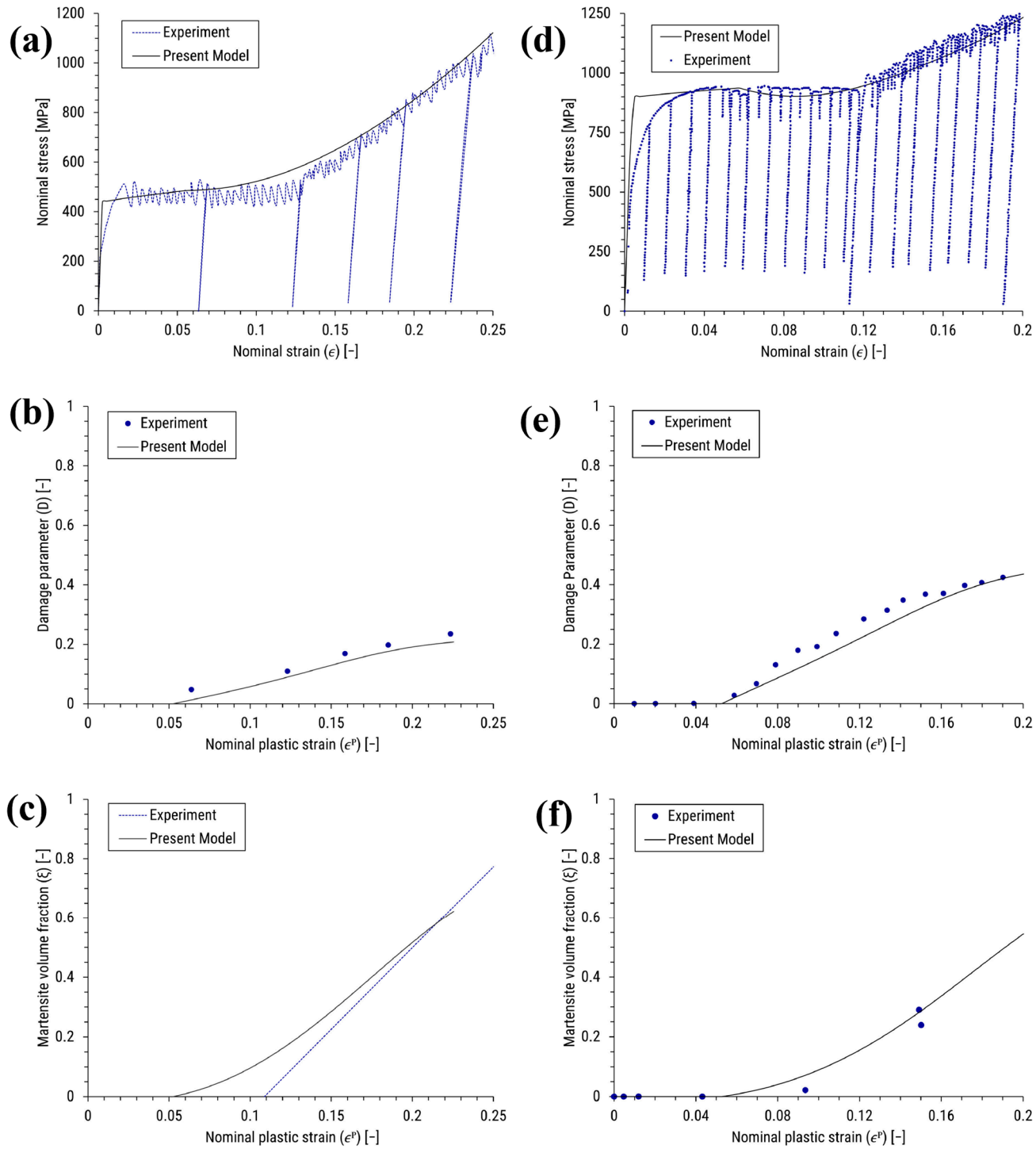

Figure 6. Comparison of constitutive model and experimental results [63] −268.8 °C stainless steel 304: (**a**) nominal stress–strain, (**b**) damage parameters D-ϵ^P, (**c**) martensitic volume fraction ξ-ϵ^P. −268.8 °C stainless steel 316L: (**d**) nominal stress–strain, (**e**) damage parameters D-ϵ^P, (**f**) martensitic volume fraction ξ-ϵ^P. Reproduced with the permission from [6], [M. Homayounfard et al.], [Int. J. Plast.]; published by [Elsevier Ltd., Amsterdam, The Netherlands], [2022].

The linear hardening reaches a critical value, which is almost ideally linear, and the value of the initial flow stress of each serration in the stress–strain curve is approximately

linear with hardening, and the elastoplastic constitutive model of linear isotropic hardening is shown in Equation (9).

$$f(\sigma_{ij}) = \sigma_i - \sigma_R(T) \tag{9}$$

- R represents the isotropic hardening parameter.
- C_R represents the hardening modulus, which is limited by Equation (10).

$$dR = C_R dp \tag{10}$$

The results of strain fracture of austenitic stainless steels at cryogenic temperatures simulated in extended finite element (XFEM) are shown in Figure 7.

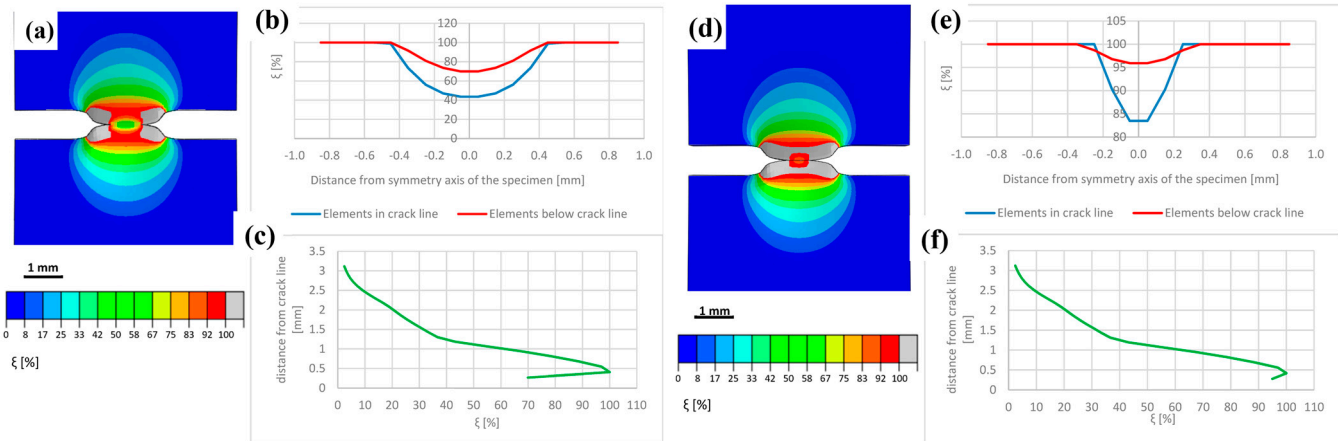

Figure 7. Martensitic volume distribution. (**a**) the strain crack growth stage at cryogenic temperatures, (**b**) the second phase distribution in the crack tips interval at the strain crack growth stage, (**c**) the martensitic distribution on the tensile axis at the strain crack growth stage, (**d**) near fracture stage at cryogenic temperatures, (**e**) the second phase distribution in the crack tips interval near the fracture stage, (**f**) the martensitic distribution on the tensile axis near fracture stage. Reprinted from Ref. [60].

The damage origin and failure of AISI 304L austenitic stainless steel during cold working was studied by a combination of experimental and numerical methods [68]. The numerical prediction of fracture in 304 stainless steel was proposed using a modified Johnson–Cook damage model [69]. A coupled elastoplastic–damage constitutive model for predicting damage in ductile materials was established using the Swift–Voce combinatorial equation as a hardening function to describe the constitutive behavior after necking [66]. The Modified Mohr–Coulomb Criterion (MMC) based on the equivalent plastic strain is used to describe the sudden fracture of 304L stainless steel plates.

There is the largest amount of martensite in the crack tips interval. The closer the distance from the tensile axis is, the less martensite there is. The farther the distance from the cross-section along the tensile axis is, the more martensite there is with an increase in phase transformation. The amount of martensite increases significantly until the tensile specimen is broken completely. At the same time, the evolution of the microstructure near the macroscopic crack growth zone at liquid nitrogen (−196 °C) and liquid helium (−268.8 °C) temperatures was determined. Accordingly, the distribution of primary and secondary phase textures at different distances from the fracture surface was experimentally analyzed, which provides a basis for the dynamics of martensitic nucleation and the constitutive relationship.

5. Conclusions

The strain of austenitic stainless steels promotes the phase transformation of austenite γ to martensite α', resulting in the increase of strength at cryogenic temperatures. The strain strengthening occurs in the temperature interval $M_s - M_d$, and the driving force

for phase transformation is $\Delta G = \Delta G_{therm} + \Delta G_{mech}$. The plastic tensile-induced phase transformation is the main mechanism.

Studies on the effect of strain on the mechanical properties of 316 steel show that the yield strength, the tensile strength, and the yield ratio increase with a decrease in experimental temperatures and an increase in pre-strain. The strength of austenitic stainless steels is significantly improved with a large elongation maintained after cyclic pre-strain at −196 °C. The effect of strain on the mechanical properties of 304 steel shows that the yield strength, the tensile strength, and the yield ratio increase to a critical value and then decrease with an increase in deformation and a decrease in experimental temperatures. This results from more dislocations interacting with newly formed nanotwins during strain.

The martensitic transformation during strain at cryogenic temperatures occurs in two ways of $\gamma \rightarrow \varepsilon \rightarrow \alpha'$ and $\gamma \rightarrow \alpha'$, where the stacking fault bundles are used as a precursor of martensite α'. In addition to the pre-existing nucleation position, the fault γ is also the nucleation position for the ε phase. The stacking fault bundle is the direct nucleation position for α' martensite. Two constitutive models for the strain strengthening of austenitic stainless steels at cryogenic temperatures are presented. One model is used to describe phase-transformation behavior during strain, and the other is used to predict fracture behavior during strain crack propagation. The calculation of the volume fraction of strain-induced martensite at cryogenic temperatures by two models is well matched with the experimental results.

Author Contributions: Methodology, J.W.; resources, B.H. and W.X.; data curation, B.H. and W.X.; writing-original draft, B.H.; writing—review and editing, J.W.; supervision, J.W. All authors have read and agreed to the published version of the manuscript.

Funding: This research was funded by the National Nature Science Foundation of China (Grant No.52075295 & No.52175305), the Nature Science Foundation of Shandong Province (Grant No. ZR2019MEE117) and Shandong University (Grant No. 2021JCG011).

Data Availability Statement: No new data were created in this study. Data sharing is not applicable to this article.

Conflicts of Interest: The authors declare no conflict of interest.

References

1. Silva, P.M.O.; Filho, M.C.C.; da Cruz, J.A.; Sales, A.J.M.; Sombra, A.S.B.; Tavares, J.M.R.S. Influence on pitting corrosion resistance of AISI 301LN and 316L stainless steels subjected to cold-induced deformation. *Metals* **2023**, *13*, 443. [CrossRef]
2. Borgioli, F. The corrosion behavior in different environments of austenitic stainless steels subjected to thermochemical surface treatments at low temperatures: An overview. *Metals* **2023**, *13*, 776. [CrossRef]
3. Lu, Y.; Hui, H. Investigation on mechanical behaviors of cold stretched and cryogenic stretched austenitic stainless steel pressure vessels. *Procedia Eng.* **2015**, *130*, 628–637. [CrossRef]
4. Li, S.; Xiao, M.; Ye, G.; Zhao, K.; Yang, M. Effects of deep cryogenic treatment on microstructural evolution and alloy phases precipitation of a new low carbon martensitic stainless bearing steel during aging. *Mater. Sci. Eng. A* **2018**, *732*, 167–177. [CrossRef]
5. Hotz, H.; Kirsch, B.; Aurich, J.C. Impact of the thermomechanical load on subsurface phase transformations during cryogenic turning of metastable austenitic steels. *J. Intell. Manuf.* **2020**, *32*, 877–894. [CrossRef]
6. Homayounfard, M.; Ganjiani, M. A large deformation constitutive model for plastic strain-induced phase transformation of stainless steels at cryogenic temperatures. *Int. J. Plast.* **2022**, *156*, 103344. [CrossRef]
7. Mazánová, V.; Heczko, M.; Škorík, V.; Chlupová, A.; Polák, J.; Kruml, T. Microstructure and martensitic transformation in 316L austenitic steel during multiaxial low cycle fatigue at room temperature. *Mater. Sci. Eng. A* **2019**, *767*, 138407. [CrossRef]
8. Zhao, Y.; Cao, Y.; Wen, W.; Lu, Z.; Zhang, J.; Liu, Y.; Chen, P. Effects of Mn content on austenite stability and mechanical properties of low Ni alumina-forming austenitic heat-resistant steel: A first-principles study. *Sci. Rep.* **2023**, *13*, 5769. [CrossRef]
9. Jiang, Y.; Zhou, X.; Li, X.; Lu, K. Stabilizing nanograined austenitic stainless steel with grain boundary relaxation. *Acta Mater.* **2023**, *256*, 119134. [CrossRef]
10. Huang, N.; Tian, Y.; Yang, R.; Xiao, T.; Li, H.; Chen, X. Effect of heat treatment on the cavitation erosion behavior of nanocrystalline surface layer of 304 stainless steel. *Appl. Sci.* **2023**, *13*, 5817. [CrossRef]
11. Fang, T.; Tao, N. Martensitic transformation dominated tensile plastic deformation of nanograins in a gradient nanostructured 316L stainless steel. *Acta Mater.* **2023**, *248*, 118780. [CrossRef]

12. Li, S.; Withers, P.J.; Kabra, S.; Yan, K. The behaviour and deformation mechanisms for 316L stainless steel deformed at cryogenic temperatures. *Mater. Sci. Eng. A* **2023**, *880*, 145279. [CrossRef]
13. Sohrabi, M.J.; Mirzadeh, H.; Sadeghpour, S.; Mahmudi, R. Dependency of work-hardening behavior of a metastable austenitic stainless steel on the nucleation site of deformation-induced martensite. *Mater. Sci. Eng. A* **2023**, *868*, 144600. [CrossRef]
14. Guo, Y.; Zhang, S.; Chen, J.; Fu, B.; Wang, Z.; Pang, L.; Wei, L.; Li, Y.; Ding, Y. The contribution of retained martensite to the high yield strength and sustainable strain hardening of a hierarchical metastable austenitic stainless steel. *Mater. Sci. Eng. A* **2023**, *866*, 144681. [CrossRef]
15. Odnobokova, M.; Belyakov, A.; Dolzhenko, P.; Kostina, M.; Kaibyshev, R. On the strengthening mechanisms of high nitrogen austenitic stainless steels. *Mater. Lett.* **2023**, *331*, 133502. [CrossRef]
16. Odnobokova, M.; Belyakov, A.; Enikeev, N.; Kaibyshev, R.; Valiev, R. Cryogenic impact toughness of a work hardened austenitic stainless steel. *Materialia* **2022**, *23*, 101460. [CrossRef]
17. Mishra, P.; Åkerfeldt, P.; Forouzan, F.; Svahn, F.; Zhong, Y.; Shen, Z.J.; Antti, M.-L. Microstructural Characterization and Mechanical Properties of L-PBF Processed 316 L at Cryogenic Temperature. *Materials* **2021**, *14*, 5856. [CrossRef]
18. Wu, S.; Xin, J.; Xie, W.; Zhang, H.; Huang, C.; Wang, W.; Zhou, Z.; Zhou, Y.; Li, L. Mechanical properties and microstructure evolution of cryogenic pre-strained 316LN stainless steel. *Cryogenics* **2021**, *121*, 103388. [CrossRef]
19. Wang, Z.; Shi, S.; Yu, J.; Li, B.; Li, Y.; Chen, X. Enhanced cryogenic tensile properties through cryogenic cyclic plastic strengthening in a metastable austenitic stainless steel. *Scr. Mater.* **2023**, *222*, 115024. [CrossRef]
20. Han, W.; Liu, Y.; Wan, F.; Liu, P.; Yi, X.; Zhan, Q.; Morrall, D.; Ohnuki, S. Deformation behavior of austenitic stainless steel at deep cryogenic temperatures. *J. Nucl. Mater.* **2018**, *504*, 29–32. [CrossRef]
21. Wolfenden, A.; Suzuki, K.; Fukakura, J.; Kashiwaya, H. Cryogenic fatigue properties of 304L and 316L stainless steels compared to mechanical strength and increasing magnetic permeability. *J. Test. Eval.* **1988**, *16*, 190. [CrossRef]
22. Bidulský, R.; Bidulská, J.; Gobber, F.S.; Kvačkaj, T.; Petroušek, P.; Actis-Grande, M.; Weiss, K.-P.; Manfredi, D. Case Study of the Tensile Fracture Investigation of Additive Manufactured Austenitic Stainless Steels Treated at Cryogenic Conditions. *Materials* **2020**, *13*, 3328. [CrossRef] [PubMed]
23. Lee, K.J.; Chun, M.S.; Kim, M.H.; Lee, J.M. A new constitutive model of austenitic stainless steel for cryogenic applications. *Comput. Mater. Sci.* **2009**, *46*, 1152–1162. [CrossRef]
24. Mallick, P.; Tewary, N.; Ghosh, S.; Chattopadhyay, P. Effect of cryogenic deformation on microstructure and mechanical properties of 304 austenitic stainless steel. *Mater. Charact.* **2017**, *133*, 77–86. [CrossRef]
25. Ma, Z.; Ren, Y.; Li, R.; Wang, Y.-D.; Zhou, L.; Wu, X.; Wei, Y.; Gao, H. Cryogenic temperature toughening and strengthening due to gradient phase structure. *Mater. Sci. Eng. A* **2017**, *712*, 358–364. [CrossRef]
26. Lu, Y.; Hui, H. Investigation on Mechanical Properties of S30403 Austenitic Stainless Steel at Different Temperatures. *J. Press. Vessel. Technol.* **2018**, *140*, 024502. [CrossRef]
27. Hauser, M.; Wendler, M.; Fabrichnaya, O.; Volkova, O.; Mola, J. Anomalous stabilization of austenitic stainless steels at cryogenic temperatures. *Mater. Sci. Eng. A* **2016**, *675*, 415–420. [CrossRef]
28. Ding, H.; Wu, Y.; Lu, Q.; Xu, P.; Zheng, J.; Wei, L. Tensile properties and impact toughness of S30408 stainless steel and its welded joints at cryogenic temperatures. *Cryogenics* **2018**, *92*, 50–59. [CrossRef]
29. Maharaja, H.; Das, B.; Singh, A.; Mishra, S. Comparative assessment of strain-controlled fatigue performance of SS 316L at room and low temperatures. *Int. J. Fatigue* **2023**, *166*, 107251. [CrossRef]
30. Ortwein, R.; Skoczeń, B.; Tock, J. Micromechanics based constitutive modeling of martensitic transformation in metastable materials subjected to torsion at cryogenic temperatures. *Int. J. Plast.* **2014**, *59*, 152–179. [CrossRef]
31. Jiang, W.; Zhu, K.; Li, J.; Qin, W.; Zhou, J.; Li, Z.; Gui, K.; Zhao, Y.; Mao, Q.; Wang, B. Extraordinary strength and ductility of cold-rolled 304L stainless steel at cryogenic temperature. *J. Mater. Res. Technol.* **2023**, *26*, 2001–2008. [CrossRef]
32. Olson, G.B.; Cohen, M. A general mechanism of martensitic nucleation: Part I. General concepts and the FCC → HCP transformation. *Met. Trans. A* **1976**, *7*, 1897–1904. [CrossRef]
33. Olson, G.B.; Cohen, M. A general mechanism of martensitic nucleation: Part II. FCC → BCC and other martensitic transformations. *Met. Trans. A* **1976**, *7*, 1905–1914. [CrossRef]
34. Van Bohemen, S.M.C. Bainite and martensite start temperature calculated with exponential carbon dependence. *Mater. Sci. Technol.* **2012**, *28*, 487–495. [CrossRef]
35. Cui, C.; Gu, K.; Qiu, Y.; Weng, Z.; Zhang, M.; Wang, J. The effects of post-weld aging and cryogenic treatment on self-fusion welded austenitic stainless steel. *J. Mater. Res. Technol.* **2022**, *21*, 648–661. [CrossRef]
36. Li, Y.; Li, J.; Ma, J.; Han, P. Influence of Si on strain-induced martensitic transformation in metastable austenitic stainless steel. *Mater. Today Commun.* **2022**, *31*, 103577. [CrossRef]
37. Pati, S.; Cohen, M. Kinetics of isothermal martensitic transformations in an iron-nickel-manganese alloy. *Acta Met.* **1971**, *19*, 1327–1332. [CrossRef]
38. Mazánová, V.; Heczko, M.; Polák, J. On the mechanism of fatigue crack initiation in high-angle grain boundaries. *Int. J. Fatigue* **2022**, *158*, 106721. [CrossRef]
39. Huang, M.; Wang, L.; Wang, C.; Mogucheva, A.; Xu, W. Characterization of deformation-induced martensite with various AGSs upon Charpy impact loading and correlation with transformation mechanisms. *Mater. Charact.* **2021**, *184*, 111704. [CrossRef]

40. Sohrabi, M.J.; Mirzadeh, H.; Sadeghpour, S.; Geranmayeh, A.R.; Mahmudi, R. Tailoring the strength-ductility balance of a commercial austenitic stainless steel with combined TWIP and TRIP effects. *Arch. Civ. Mech. Eng.* **2023**, *23*, 170. [CrossRef]
41. Injeti, V.; Li, Z.; Yu, B.; Misra, R.; Cai, Z.; Ding, H. Macro to nanoscale deformation of transformation-induced plasticity steels: Impact of aluminum on the microstructure and deformation behavior. *J. Mater. Sci. Technol.* **2018**, *34*, 745–755. [CrossRef]
42. Alves, C.L.M.; Rezende, J.; Senk, D.; Kundin, J. Peritectic phase transformation in the Fe–Mn and Fe–C system utilizing simulations with phase-field method. *J. Mater. Res. Technol.* **2019**, *8*, 233–242. [CrossRef]
43. Tian, Y.; Lienert, U.; Borgenstam, A.; Fischer, T.; Hedström, P. Martensite formation during incremental cooling of Fe-Cr-Ni alloys: An in-situ bulk X-ray study of the grain-averaged and single-grain behavior. *Scr. Mater.* **2017**, *136*, 124–127. [CrossRef]
44. Masumura, T.; Nakada, N.; Tsuchiyama, T.; Takaki, S.; Koyano, T.; Adachi, K. The difference in thermal and mechanical stabilities of austenite between carbon- and nitrogen-added metastable austenitic stainless steels. *Acta Mater.* **2015**, *84*, 330–338. [CrossRef]
45. Ruan, T.; Wang, B.; Li, Y.; Xu, C. Atomistic insight into the solid-solid phase transitions in iron nanotube: A molecular dynamics study. *Mater. Today Commun.* **2021**, *29*, 102833. [CrossRef]
46. Zeng, L.; Song, X.; Chen, N.; Rong, Y.; Zuo, X.; Min, N. A new understanding of transformation induced plasticity (TRIP) effect in austenitic steels. *Mater. Sci. Eng. A* **2022**, *857*, 143742. [CrossRef]
47. Wang, J.; Xi, X.; Li, Y.; Wang, C.; Xu, W. New insights on nucleation and transformation process in temperature-induced martensitic transformation. *Mater. Charact.* **2019**, *151*, 267–272. [CrossRef]
48. Wang, T.; Wei, X.; Zhang, H.; Ren, Z.; Gao, B.; Han, J.; Bian, L. Plastic deformation mechanism transition with solute segregation and precipitation of 304 stainless steel foil induced by pulse current. *Mater. Sci. Eng. A* **2022**, *840*, 142899. [CrossRef]
49. Liu, T.; Liang, L.; Raabe, D.; Dai, L. The martensitic transition pathway in steel. *J. Mater. Sci. Technol.* **2023**, *134*, 244–253. [CrossRef]
50. Galindo-Nava, E.; Rivera-Díaz-Del-Castillo, P. Understanding martensite and twin formation in austenitic steels: A model describing TRIP and TWIP effects. *Acta Mater.* **2017**, *128*, 120–134. [CrossRef]
51. Moallemi, M.; Kermanpur, A.; Najafizadeh, A.; Rezaee, A.; Baghbadorani, H.S.; Nezhadfar, P.D. Deformation-induced martensitic transformation in a 201 austenitic steel: The synergy of stacking fault energy and chemical driving force. *Mater. Sci. Eng. A* **2016**, *653*, 147–152. [CrossRef]
52. Stringfellow, R.; Parks, D.; Olson, G. A constitutive model for transformation plasticity accompanying strain-induced martensitic transformations in metastable austenitic steels. *Acta Metall. Mater.* **1992**, *40*, 1703–1716. [CrossRef]
53. Garion, C.; Skoczen, B. Modeling of plastic strain-induced martensitic transformation for cryogenic applications. *J. Appl. Mech.* **2002**, *69*, 755–762. [CrossRef]
54. Garion, C.; Skoczen, B. Combined model of strain-induced phase transformation and orthotropic damage in ductile materials at cryogenic temperatures. *Int. J. Damage Mech.* **2003**, *12*, 331–356. [CrossRef]
55. Ryś, M.; Egner, H. Energy equivalence based constitutive model of austenitic stainless steel at cryogenic temperatures. *Int. J. Solids Struct.* **2019**, *164*, 52–65. [CrossRef]
56. Homayounfard, M.; Ganjiani, M.; Sasani, F. Damage development during the strain induced phase transformation of austenitic stainless steels at low temperatures. *Model. Simul. Mater. Sci. Eng.* **2021**, *29*, 045004. [CrossRef]
57. Xie, L.; Zhang, H.; Wu, S.; Shen, F.; Xin, J.; Huang, C.; Jiang, M.; Huang, Z.; Wang, W.; Li, L. Development of two-dimensional temperature field solution method based on the stress–strain response of 316LN stainless steel at cryogenic temperatures. *Cryogenics* **2023**, *133*, 103713. [CrossRef]
58. Wei, Y.; Lu, Q.; Kou, Z.; Feng, T.; Lai, Q. Microstructure and strain hardening behavior of the transformable 316L stainless steel processed by cryogenic pre-deformation. *Mater. Sci. Eng. A* **2023**, *862*, 144424. [CrossRef]
59. Chen, L.; Jia, Q.; Hao, S.; Wang, Y.; Peng, C.; Ma, X.; Zou, Z.; Jin, M. The effect of strain-induced martensite transformation on strain partitioning and damage evolution in a duplex stainless steel with metastable austenite. *Mater. Sci. Eng. A* **2021**, *814*, 141173. [CrossRef]
60. Nalepka, K.; Skoczeń, B.; Ciepielowska, M.; Schmidt, R.; Tabin, J.; Schmidt, E.; Zwolińska-Faryj, W.; Chulist, R. Phase transformation in 316L austenitic steel induced by fracture at cryogenic temperatures: Experiment and modelling. *Materials* **2021**, *14*, 127. [CrossRef]
61. Egner, H.; Skoczeń, B.; Ryś, M. Constitutive and numerical modeling of coupled dissipative phenomena in 316L stainless steel at cryogenic temperatures. *Int. J. Plast.* **2015**, *64*, 113–133. [CrossRef]
62. Ryś, M.; Skoczeń, B. Coupled constitutive model of damage affected two-phase continuum. *Mech. Mater.* **2017**, *115*, 1–15. [CrossRef]
63. Tabin, J.; Skoczen, B.; Bielski, J. Damage affected discontinuous plastic flow (DPF). *Mech. Mater.* **2017**, *110*, 44–58. [CrossRef]
64. Li, Y.; Zhong, S.; Luo, H.; Xu, C.; Jia, X. Intermediate stacking fault and twinning induced cooperative strain evolution of dual phase in lean duplex stainless steels with excellent cryogenic strength-ductility combinations. *Mater. Sci. Eng. A.* **2022**, *831*, 142347. [CrossRef]
65. Paredes, M.; Grolleau, V.; Wierzbicki, T. On ductile fracture of 316L stainless steels at room and cryogenic temperature level: An engineering approach to determine material parameters. *Materialia* **2020**, *10*, 100624. [CrossRef]
66. Kim, M.-S.; Kim, H.-T.; Choi, Y.-H.; Kim, J.-H.; Kim, S.-K.; Lee, J.-M. A New Computational Method for Predicting Ductile Failure of 304L Stainless Steel. *Metals* **2022**, *12*, 1309. [CrossRef]
67. Tabin, J.; Skoczen, B.; Bielski, J. Discontinuous plastic flow coupled with strain induced fcc–bcc phase transformation at extremely low temperatures. *Mech. Mater.* **2019**, *129*, 23–40. [CrossRef]

68. Ben Othmen, K.; Haddar, N.; Jegat, A.; Manach, P.-Y.; Elleuch, K. Ductile fracture of AISI 304L stainless steel sheet in stretching. *Int. J. Mech. Sci.* **2019**, *172*, 105404. [CrossRef]
69. Pham, H.T.; Iwamoto, T. An evaluation of fracture properties of type-304 austenitic stainless steel at high deformation rate using the small punch test. *Int. J. Mech. Sci.* **2018**, *144*, 249–261. [CrossRef]